Available online at www.sciencedirect.com
SCIENCE DIRECT®
Journal of Sound and Vibration 280 (2005) 159–179
JOURNAL OF SOUND AND VIBRATION
www.elsevier.com/locate/jsvi

Experimental energetic analyses of an actively controlled one-dimensional acoustic waveguide

L.V. Donadon, J.R.F. Arruda*

DMC/FEM/UNICAMP, Caixa postal 6122, Campinas, São Paulo CEP 13083-970, Brazil

Received 18 March 2002; accepted 3 December 2003

Abstract

Technological development has made it possible to implement digital active noise control systems in real time. This work compares the performance of different adaptive control methods applied to a one-dimensional waveguide. The compared control methods are the frequency-domain filtered-X LMS using potential energy density and kinetic energy density as cost functions, and the active sound intensity control (ASIC), which uses active intensity as the cost function. The ASIC controller is implemented with both the P–U approach (measuring pressure and particle velocity at the same time) and the P–P approach (using two microphones to estimate the active intensity). The waveguide is a circular PVC duct with a primary source placed at one end, the secondary source placed near the mid-span of the duct, and with an open-ended termination. The analyses were performed comparing the results in terms of the potential energy density, the active intensity, and the acoustic power radiated by the sources. Moreover, it is shown how to choose suitable error sensors and their influence in the performance of the ASIC controller. The results show that the control methods achieved the same final result and, as expected, when the volume velocity of the secondary source was driven to the optimal volume velocity, the primary source and the secondary source radiated less acoustic power than the uncontrolled primary source. Besides, the sound intensity was effectively attenuated throughout the duct.

1. Introduction

Lately, there have been several studies about methods that use intensity as the cost function. Sommerfeldt and Nashif [1] used a method based upon the filtered-X LMS algorithm, where the adaptive updating of the filter weights is done in the time domain, thus minimizing both the active and reactive power components. Kang and Kim [2] also used a method based upon the filtered-X

*Corresponding author. Tel.: +55-19-3788-3194; fax: +55-19-3289-3722.
E-mail addresses: lazaro@fem.unicamp.br (L.V. Donadon), arruda@fem.unicamp.br (J.R.F. Arruda).

0022-460X/$ - see front matter © 2004 Elsevier Ltd. All rights reserved.
doi:10.1016/j.jsv.2003.12.024

LMS algorithm, where the gradient of the product of the instantaneous pressure and particle velocity is computed using an intensity probe, again in the time domain.

Qiu and Hansen [3] used the intensity in the frequency domain as cost function, but there is no reference signal in their method. Because of this, the controller will try to cancel all the sound intensity in the environment, not only the intensity that is coherent with the reference signal.

Swanson et al. [4] used the filtered-X LMS in the frequency domain as an active intensity control method by replacing pressure for intensity as the error signal. The transfer function between the reference signal and the measured active intensity is used as the filtered path. In their implementation, the control signal is obtained by time filtering of the reference signal using weights obtained by the inverse Fourier transform of the frequency-domain weights computed by the algorithm. The transfer function of the error path, in this case the active intensity transfer function between the error sensors and the secondary source, is identified on-line in the frequency domain. This control path filtering is the most controversial part of the algorithm, as acknowledged by the authors.

Arruda et al. [5] used the active intensity as the cost function to control the energy flow in plates. This method has been compared with the frequency-domain filtered-X LMS [6] by Pereira et al. [7] and Donadon et al. [8]. The comparison was performed using a theoretical duct example.

The aim of this work is to experimentally compare the performance of several active noise control (ANC) methods. The compared methods are based upon controlling the potential energy density, the kinetic energy density, the active intensity using the two-microphone technique, and the active intensity using a microphone and a particle velocity sensor. The methods were implemented in the frequency domain, where there is the possibility of controlling each frequency line independently, in their normalized version, which allows the same convergence rate at all frequencies. The paper addresses experimental issues such as the influence of the phase mismatch error and the use of particle velocity error sensors in ANC applications.

2. Control equations

The control methods were developed for the 1–1–1 case, i.e., one primary source, one secondary source and one error sensor, using an adaptive filtering technique in a feedforward configuration [6]. All the equations presented here are developed in the frequency domain. It is relatively straightforward to generalize the formulations for multiple channel cases.

2.1. Pressure and velocity equations

The control methods will be applied to a one-dimensional waveguide, where x represents the spatial co-ordinate along which propagation takes place.

Considering firstly a plane wave source acting in an acoustic one-dimensional waveguide with a given volume velocity Q, the pressure P and the particle velocity u at any location in the field can be evaluated as

$$P(x, x_0) = Z(x, x_0)Q, \quad u(x, x_0) = Y(x, x_0)Q, \tag{1}$$

where Z is the "transfer" acoustic impedance, $Z = P/Q$, Y is the "transfer" acoustic mobility, $Y = u/Q$, for a source located at position x_0 and the pressure measured at position x.

Now, consider the case where two sources are acting in the acoustic field. One primary source, the source that originally emits the noise, represented by the subscript $_P$, and one secondary source, the source added to the acoustic field in order to attenuate the noise generated by the primary source, represented by the subscript $_S$. Thus, the total pressure P_T, can be written as

$$P_T = Z_P Q_P + Z_S Q_S, \tag{2}$$

where $P_T \equiv P(x, x_P, x_S), Z_P \equiv Z(x, x_P), Z_S \equiv Z(x, x_S)$, x_P is the primary source position, and x_S is the secondary source position. The pressure field generated by the primary source is $P_P \equiv P(x, x_P) = Z_P Q_P$, and the pressure field generated by the secondary source is $P_S \equiv P(x, x_S) = Z_S Q_S$.

In the same way as the pressure field, the total particle velocity u_T generated by the two sources in the field can be written as

$$u_T = Y_P Q_P + Y_S Q_S, \tag{3}$$

where $u_T \equiv u(x, x_P, x_S)$, $Y_P \equiv Y(x, x_P)$ and $Y_S \equiv Y(x, x_S)$. The velocity field generated by the primary source is $u_P \equiv u(x, x_P) = Y_P Q_P$, and the velocity field generated by the secondary source is $u_S \equiv u(x, x_S) = Y_S Q_S$.

In order to simplify the notation, positions x, x_S and x_P will be omitted unless where necessary for the understanding of the equations. Besides, it is important to remember that the total particle velocity, Eq. (3), has a direction, given by its sign in the one-dimensional waveguide case.

2.2. Adaptive filter equations

The control methods presented here are based upon the feedforward adaptive filter theory [6], which consists of filtering the reference by a finite impulse response (FIR) filter and using the resulting signal as the control signal. The reference signal is correlated with the error signal and contains information about frequency and phase of the noise generated by the primary source. Without loss of generality, the reference is represented by the volume velocity from the primary source, Q_P. The control law is represented by the volume velocity from the secondary source, Q_S. So, the volume velocity from the secondary source is evaluated as

$$Q_S = W Q_P, \tag{4}$$

where W is a weight function which will be found recursively by an adaptive law.

The adaptive law will be developed using a self-orthogonalizing adaptive filtering algorithm as [6,9]

$$W(n+1) = W(n) - \mu R^{-1} \nabla J(n), \tag{5}$$

where n is the iteration time, μ is the step-size defined between 0 and 1, R^{-1} is the inverse of a correlation matrix R, and $\nabla J(n)$ is the gradient of the cost function at iteration n. R and ∇J will be outlined for each control method depending on each cost function.

Eq. (5) is a modified formulation of the steepest-descent method, which is more suitable in control applications because the step-size μ is independent of the eigenvalues of the correlation

matrix R. Besides, when formulated in the frequency domain, it guarantees a constant rate of convergence for all frequency lines [6,9].

2.3. Adaptive control method based upon controlling the potential energy density

The potential energy density, E_P, is related to the change in volume when the acoustic wave propagates, and is given by [10]

$$E_P = \frac{1}{2\rho c^2}|P|^2, \tag{6}$$

where ρ is the air density, and c is the sound speed.

Using E_P as cost function, and substituting Eqs. (2) and (4) in Eq. (6), the cost function becomes

$$J = E_P = \frac{1}{2\rho c^2}|Z_P Q_P + Z_S W Q_P|^2. \tag{7}$$

Taking the gradient of Eq. (7) in relation to W, it is easy to find

$$\nabla J = \frac{1}{2\rho c^2}\, 2(Z_S Q_P)^* P_T, \tag{8}$$

where * denotes the complex conjugate.

The correlation matrix R will be found as in Ref. [11]. So, expanding Eq. (8) and using Eqs. (2) and (4),

$$\nabla J = \frac{1}{2\rho c^2}\, 2(Z_S Q_P)^*(Z_P Q_P + Z_S W Q_P). \tag{9}$$

The correlation matrix R is the term that multiplies the weight function W,

$$R = \frac{1}{2\rho c^2}\, 2(Z_S Q_P)^* Z_S Q_P = \frac{1}{\rho c^2}|Z_S Q_P|^2. \tag{10}$$

Finally, taking the results in Eqs. (10) and (8) and substituting them in Eq. (5), the adaptive control method that minimizes the potential energy density becomes

$$W(n+1) = W(n) - \mu \frac{(Z_S Q_P)^*}{|Z_S Q_P|^2} P_T. \tag{11}$$

Eq. (11) is known as the frequency-domain filtered-X LMS [6] in its normalized version. It must be assured that the denominator of Eq. (11) will not vanish, which will not happen provided the error sensor, in this case a microphone, ''sees'' some response from the secondary source. The method will adapt until the numerator is equal to zero, which happens if total pressure P_T is equal to zero. Therefore, the optimal volume velocity of the secondary source can be found by making the total pressure equal to zero, resulting in

$$Q_S = -\frac{Z_P}{Z_S} Q_P. \tag{12}$$

Eq. (12) represents the best performance that the frequency-domain filtered-X LMS based upon controlling potential energy density can achieve [12]. This method will be named in shorthand notation as LMS-P.

The LMS-P can be successfully implemented where the pressure sensor (a microphone) can give good signal levels to be used as an error sensor, which will not happen if the microphone is placed at a pressure node.

2.4. Adaptive control method based upon controlling the kinetic energy density

The kinetic energy density, E_K, is related to the particle velocity in the acoustic field and is given by [10]

$$E_K = \tfrac{1}{2}\,\rho|u|^2. \tag{13}$$

Thus, it is noted that the equations to control E_K are analogous to the equations to control E_P, but with Z replaced by Y. Thus, the adaptive control method which minimizes the kinetic energy density is evaluated using Eq. (11) by replacing Z by Y and P_T by u_T,

$$W(n+1) = W(n) - \mu\,\frac{(Y_S Q_P)^*}{|Y_S Q_P|^2}\,u_T. \tag{14}$$

Thus, the method presented in Eq. (14) is the same frequency-domain filtered-X LMS but now based upon controlling the kinetic energy density. The same observations about the convergence made for Eq. (11) are valid for Eq. (14), where it is necessary for the particle velocity sensor to "see" some response from the secondary source. The optimal volume velocity controlling the kinetic energy density is evaluated as [12]

$$Q_S = -\frac{Y_P}{Y_S}\,Q_P. \tag{15}$$

Eq. (15) represents the best performance that the frequency-domain filtered-X LMS based upon controlling the kinetic energy density can achieve [12]. This method will be named in shorthand notation as LMS-U.

The kinetic energy density has already been used as cost function in previous works together with the potential energy density cost function, forming the energy density cost function ($E_P + E_K$) [1,13]. While, in these previous works, the kinetic energy density control was implemented in the time domain and the particle velocity was estimated using the two-microphone approach [14], here the kinetic energy density control is implemented in the frequency domain and using a "true" particle velocity sensor, which will be described in Section 3.

2.5. Adaptive control method based upon controlling the active intensity using the P–U approach

The active intensity is related to the energy flow and only exists if the pressure and particle velocity measured at the same point are not in the phase quadrature, or, simply, if there is dissipation in the acoustic field, which can be caused, for instance, by a radiation impedance at the end of the duct. The active intensity, I_A, using the P–U approach is defined as [14]

$$I_A = \tfrac{1}{2}\,\Re\{Pu^*\}, \tag{16}$$

where $\Re$ indicates the real part of a complex quantity. Generally speaking, the active intensity is a vectorial quantity, but, for a one-dimensional waveguide, it is a scalar, its sign indicating a positive or negative direction. However, to simplify the development, given that the control point will be past the primary and secondary sources, towards the end of the duct, the active intensity will always be positive and can be used as a suitable function [1,3].

Using I_A as the cost function and substituting Eqs. (2)–(4) in Eq. (16),

$$J = I_A = \tfrac{1}{2}\,\Re\{(Z_P Q_P + Z_S W Q_P)(Y_P Q_P + Y_S W Q_P)^*\}. \tag{17}$$

Taking the gradient of Eq. (17) in relation to W, it is easy, with some algebraic manipulation, to find

$$\nabla J = \tfrac{1}{2}(Y_S Q_P)^* P_T + \tfrac{1}{2}(Z_S Q_P)^* u_T. \tag{18}$$

Now, the correlation matrix R is found expanding Eq. (18) using Eqs. (2)–(4), and taking the term that multiplies W:

$$\nabla J = \tfrac{1}{2}(Y_S Q_P)^* Z_P Q_P + \tfrac{1}{2}(Z_S Q_P)^* Y_P Q_P + \tfrac{1}{2}(Y_S Q_P)^* Z_S W Q_P + \tfrac{1}{2}(Z_S Q_P)^* Y_S W Q_P. \tag{19}$$

Thus, the correlation matrix R is given by

$$R = \tfrac{1}{2}(Y_S Q_P)^* Z_S Q_P + \tfrac{1}{2}(Z_S Q_P)^* Y_S Q_P = \Re\{Z_S Q_P (Y_S Q_P)^*\}. \tag{20}$$

Finally, the adaptive method which effectively minimizes the active intensity using the P–U approach is found substituting Eqs. (19) and (20) into Eq. (5),

$$W(n+1) = W(n) - \frac{\mu}{2}\frac{(Y_S Q_P)^* P_T + (Z_S Q_P)^* u_T}{\Re\{Z_S Q_P (Y_S Q_P)^*\}}. \tag{21}$$

It should be noted that the adaptive control method proposed in Eq. (21) will have convergence problems if the denominator is close to zero. This denominator is proportional to the active intensity from the secondary source measured with the P–U approach, since $Z_S Q_P$ and $Y_S Q_P$ give information about pressure and particle velocity from the secondary source, respectively. Thus, it is necessary for the error sensor to "see" some active intensity from the secondary source. Otherwise, the measured intensity cannot be controlled with the secondary source (controllability problem). The method will adapt until the numerator is equal to zero, which will happen if the volume velocity of the secondary source is given by [12]

$$Q_S = -\frac{Y_S^* Z_P + Z_S^* Y_P}{2\Re\{Z_S Y_S^*\}}\, Q_P. \tag{22}$$

Eq. (22) represents the best performance the method that controls the active intensity using the P–U approach can achieve [12]. This method will be named in shorthand notation as ASIC-PU, and a more detailed formulation of this method can be found in Ref. [15].

The equations presented above are the explicit formulation of the controller using the active intensity as a cost function. It is basically the same controller proposed by Swanson et al. [4] but the derivation of Eqs. (21) and (22) allowed the analysis of the algorithm in much more detail.

2.6. Adaptive control method based upon controlling the active intensity using the P–P approach

The active intensity using the P–P approach is measured using two microphones spaced by δ in the acoustic field. The measured intensity component will be the component in the direction defined by the two microphones [14]. Using P_1 and P_2 to represent the measured pressures at positions 1 and 2, respectively, the pressure at the position between the microphones, represented by P_{12}, can be evaluated as

$$P_{12} \cong \frac{P_1 + P_2}{2}, \tag{23}$$

where

$$P_1 = Z_{P1} Q_P + Z_{S1} Q_S, \quad P_2 = Z_{P2} Q_P + Z_{S2} Q_S, \tag{24}$$

with $Z_{P1} \equiv Z(x_1, x_P), Z_{P2} \equiv Z(x_2, x_P), Z_{S1} \equiv Z(x_1, x_S)$, and $Z_{S2} \equiv Z(x_2, x_S)$.

The particle velocity is obtained approximating the spatial pressure gradient by first order finite differences,

$$\nabla P \cong \frac{P_2 - P_1}{\delta}. \tag{25}$$

So, the particle velocity evaluated at the position between the microphones, u_{12}, is given by

$$u_{12} = \frac{\mathrm{i}}{\omega\rho} \frac{P_2 - P_1}{\delta}, \tag{26}$$

where i is the imaginary number.

Therefore, the active intensity using the P–P approach is given by [14]

$$I_A = \tfrac{1}{2} \Re\{P_{12} u_{12}^*\} = \frac{1}{4\omega\rho\delta} \Re\{\mathrm{i}(|P_1|^2 - P_1 P_2^* + P_2 P_1^* - |P_2|^2)\} = \frac{1}{2\omega\rho\delta} \Im\{P_1 P_2^*\}. \tag{27}$$

Now, using Eq. (27) as the cost function, substituting Eq. (24),

$$J = I_A = \frac{1}{2\omega\rho\delta} \Im\{(Z_{P1} Q_P + Z_{S1} W Q_P)(Z_{P2} Q_P + Z_{S2} W Q_P)^*\}. \tag{28}$$

Taking the gradient of each term of Eq. (28) in relation to W,

$$\begin{aligned}
&\nabla \Im\{(Z_{P2} Q_P)^* Z_{P1} Q_P\} = 0,\\
&\nabla \Im\{(Z_{P2} Q_P)^* Z_{S1} W Q_P\} = \mathrm{i}(Z_{S1} Q_P)^* Z_{P2} Q_P,\\
&\nabla \Im\{(Z_{S2} W Q_P)^* Z_{P1} Q_P\} = -\mathrm{i}(Z_{S2} Q_P)^* Z_{P1} Q_P,\\
&\nabla \Im\{(Z_{S2} W Q_P)^* Z_{S1} W Q_P\} = \mathrm{i}(Z_{S1} Q_P)^* Z_{S2} W Q_P - \mathrm{i}(Z_{S2} Q_P)^* Z_{S1} W Q_P
\end{aligned} \tag{29}$$

with some algebraic manipulation it is easy to find

$$\nabla J = \frac{\mathrm{i}}{2\omega\rho\delta}[(Z_{S1} Q_P)^* P_2 - (Z_{S2} Q_P)^* P_1]. \tag{30}$$

The correlation matrix R is found by expanding Eq. (30) with Eqs. (2)–(4), therefore

$$\nabla J = \frac{\mathrm{i}}{2\omega\rho\delta}[(Z_{S1} Q_P)^* (Z_{P2} Q_P + Z_{S2} W Q_P) - (Z_{S2} Q_P)^* (Z_{P1} Q_P + Z_{S1} W Q_P)], \tag{31}$$

where the correlation matrix R is the term that multiplies W,

$$R = \frac{\mathrm{i}}{2\omega\rho\delta}[(Z_{S1}Q_P)^* Z_{S2}Q_P - (Z_{S2}Q_P)^* Z_{S1}Q_P] = \frac{1}{2\omega\rho\delta}\,\Im\{Z_{S1}Q_P(Z_{S2}Q_P)^*\}. \tag{32}$$

Finally, the method that controls the active intensity using the P–P approach is obtained by substituting Eqs. (30) and (32) in Eq. (5),

$$W(n+1) = W(n) - \frac{\mathrm{i}\mu}{2}\frac{(Z_{S1}Q_P)^* P_2 - (Z_{S2}Q_P)^* P_1}{\Im\{Z_{S1}Q_P(Z_{S2}Q_P)^*\}}. \tag{33}$$

Eq. (33) represents the method derived in Refs. [16,17] for structural intensity control and applied to a duct with plane wave approach [7, 8]. This method will be named in shorthand notation ASIC-PP, and a more detailed formulation of this method can be found in Ref. [15].

It should be noted that the control method expressed in Eq. (33) may have convergence problems if the denominator is close to zero. This denominator is proportional to the active intensity from the secondary source measured by the P–P approach. Thus, it is necessary for the error sensor to "see" some active intensity from the secondary source (controllability). The method can be adapted until the numerator vanishes, which will happen if the volume velocity of the secondary source is given by

$$Q_S = \frac{Z_{S1}^* Z_{P2} - Z_{S2}^* Z_{P1}}{2\mathrm{i}\Im\{Z_{S1}Z_{S2}^*\}}\,Q_P. \tag{34}$$

Eq. (34) represents the best performance that this method, which controls the active intensity using the P–P approach, can achieve.

It is important to note that the controllers proposed in Eqs. (21) and (33) were designed using the active intensity as the cost function, but it is known that the active intensity can be either positive or negative. Thus, the cost function is not quadratic, which means that the control method can become unstable. However, Eq. (33) expresses the same result shown by Arruda and Perreira [17], where the squared active intensity is the cost function, in which case there is a global minimum. Therefore, the final result using the active intensity and its squared value as the cost function are the same for a scalar intensity. This happens because of the normalization made in both cases [17].

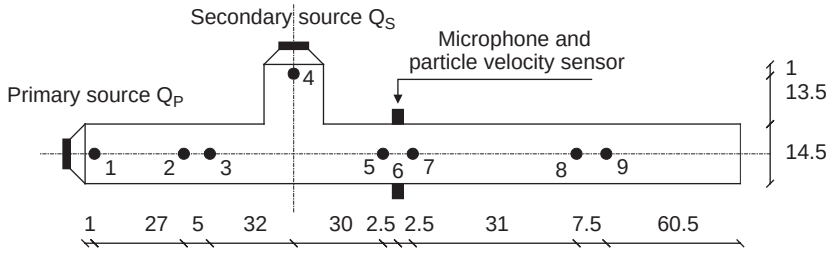

Fig. 1. Position of sensors and actuators in the duct. Lengths are in centimeters.

3. Experimental setup

The Experimental setup is shown in Fig. 1. It consists of a 6″ diameter circular section PVC duct with 2 loudspeakers. At all locations represented by subscripts 1–9, omnidirectional 1/4″ microphones were placed, except for position 6, where a particle velocity sensor and a microphone were placed.

The duct configuration presented in Fig. 1 enables: the measurement of the radiated acoustic power from the sources using microphones located at positions 1 and 4; the measurement of the active intensity upstream and downstream the secondary source with the P–P approach using the microphones at positions 2 and 3 and at positions 8 and 9; the control of the potential energy density at position 5 using the LMS-P approach; the control of the kinetic energy density at position 6 using the LMS-U approach; the control of the active intensity at position 6 using the P–U approach (ASIC-PU), and the control of the active intensity at position 6 using the P–P approach (ASIC-PP) with the microphones at positions 5 and 7.

The particle velocity used in the ASIC-PU and LMS-U methods can be measured using a particle velocity sensor that has been developed by Microflown Technologies [18–20]. The position of the particle velocity sensor is indicated in Fig. 1. It is placed between the microphones at positions 5 and 7. This sensor consists basically of two hot wires which are exposed to the air flow caused by the acoustic pressure oscillation. When the sensor is exposed to an acoustic field, the difference in temperature between the upstream and downstream hot wires is proportional to the particle velocity. The velocity sensor used in this work is the U-probe model I, which is ICP-driven and with a 1/2″ casing, designed to measure the particle velocity in one direction. The sensibility of the particle velocity sensor is highly dependent on frequency, and calibration is more involved than with conventional microphones [21].

The controllers were developed in Matlab/Simulink and implemented in real time using a dSPACE 1102 control board with 16 weights in frequency and with a sample rate of 1.5 ms. The step-size μ was changed on-line to promote a better adaptation rate.

The electrical signal used to drive the primary source was a saw-tooth with a fundamental frequency of 41.66 Hz. After being generated, the electrical signal was filtered by an analog filter with a roll-off of 48 dB per decade of attenuation and cut-off frequency of 110 Hz. Therefore, only the frequencies 41.66, 83.33 and 125 Hz were excited. A general block diagram can be found in Fig. 2.

An analog low-pass filter with 180 Hz of cut-off frequency was used to reconstruct the digital control signal generated by the D/A converter of the dSPACE 1102 control board, and a block diagram can be seen in Fig. 3.

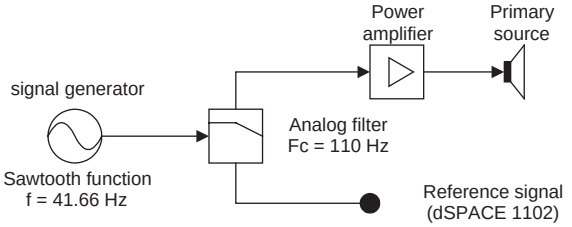

Fig. 2. Block diagram of the excitation system.

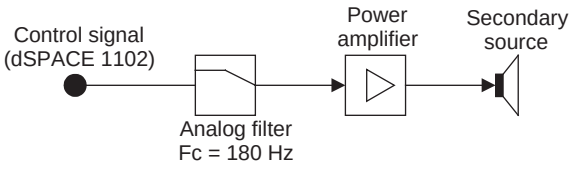

Fig. 3. Block diagram of the control signal.

3.1. Experimental measurements of the acoustical properties

The acoustic power radiated from the sources can be evaluated by measuring the total pressure immediately in front of the source and the volume velocity of the source as [22]

$$W_R = \tfrac{1}{2}\,\Re\{PQ^*\} = \Re\{G_{QP}\}, \tag{35}$$

where P is the measured pressure immediately in front of the source, Q is the volume velocity imposed by the source and G_{QP} is the crosspower between the volume velocity and pressure.

In order to measure the radiated acoustic power properly, the microphones at positions 1 and 4 were placed as close as possible to the sources, and the volume velocities of the sources were measured using a laser Doppler vibrometer, which measured the velocity of the loudspeaker cone. The Doppler signal was improved by using a retro-reflective tape on the loudspeaker cone. Thus, the acoustic power radiated by the primary source is calculated as

$$W_{RP} = \tfrac{1}{2}\,\Re\{P_1 u(x_P)^* S\} = \tfrac{1}{2}\,\Re\{P_1 Q_P^*\} = \Re\{G_{Q_{PP1}}\}, \tag{36}$$

where $u(x_P)$ is the particle velocity of the primary source measured by the laser vibrometer and S is the duct area. The acoustic power radiated by the secondary source is calculated as

$$W_{RS} = \tfrac{1}{2}\,\Re\{P_4 u(x_S)^* S\}\tfrac{1}{2}\,\Re\{P_4 Q_S^*\} = \Re\{G_{Q_S P_4}\}, \tag{37}$$

where $u(x_S)$ is the particle velocity of the secondary source measured by the laser vibrometer.

It should be noted that nearfield effects close to the loudspeaker due to the non-ideal movement of the cone, can influence the estimated acoustic power. However, such effects are expected to be small for a $6''$ loudspeaker in the frequency range of the experiments.

The active intensity can be evaluated using the P–P approach as [14]

$$I_A = \frac{1}{2\omega\rho\delta}\,\Im\{P_1 P_2^*\} = \frac{1}{\omega\rho\delta}\,\Im\{G_{P2P1}\}, \tag{38}$$

where G_{P2P1} is the crosspower between the two microphones placed close to each other, and δ is the separation distance between them.

However, the method of measuring the active intensity using the P–P approach, Eq. (38), is subject to many errors [14]. Among them, the systematic error due to phase mismatch between the two microphones can be highlighted, which can become critical when performing the intensity measurement in a reverberant field or when the two microphones are placed very close to each other in order to minimize the error due to the finite difference approximation.

The phase mismatch can be minimized by using a "geometric mean" in the crosspower between the sensors as [23]

$$\tilde{G}_{P2P1} = \sqrt{{}_s G_{P2P1} G_{P2P1}}, \tag{39}$$

where G_{P2P1} is the crosspower with the sensors in the original order and ${}_sG_{P2P1}$ is the crosspower with the sensors in the switched order. The necessity of phase correction can be observed more clearly in Section 3.2, where the microphones used in the control application are analyzed and the phase mismatch between the microphones is shown.

The finite difference approximation error correction can be overcome as proposed in Ref. [24] by multiplying the crosspower by a correction factor given by

$$\frac{k\delta}{\sin(k\delta)} = \frac{1}{\mathrm{sinc}(k\delta)}, \tag{40}$$

where k is the wavenumber and δ is the separation distance between the sensors. Eq. (40) is the velocity correction factor for plane waves caused by the approximation of the pressure gradient by the finite differences.

Thus, the active intensity using the P–P principle with the error correction of Eqs. (39) and (40) can be expressed as

$$I_A = \frac{1}{\omega\rho\delta}\frac{k\delta}{\sin(k\delta)}\,\Im\{\tilde{G}_{P2P1}\}. \tag{41}$$

Therefore, the active intensity between microphones placed at positions 2 and 3, I_{A23}, is given by

$$I_{A23} = \frac{1}{2\omega\rho\delta}\,\Im\{P_2P_3^*\} = \frac{1}{\omega\rho\delta}\frac{k\delta}{\sin(k\delta)}\,\Im\{\tilde{G}_{P3P2}\}, \tag{42}$$

where P_2 and P_3 are the pressures measured at positions 2 and 3, respectively, δ is the separation distance between the microphones, and $\tilde{G}_{P3P2}$ is the crosspower corrected for phase mismatch. The active intensity flowing through the sensors 8 and 9, I_{A89}, is given by

$$I_{A89} = \frac{1}{2\omega\rho\delta}\,\Im\{P_8P_9^*\} = \frac{1}{\omega\rho\delta}\frac{k\delta}{\sin(k\delta)}\,\Im\{\tilde{G}_{P9P8}\}, \tag{43}$$

where P_8 and P_9 are the pressures measured at position 8 and 9, respectively, and $\tilde{G}_{P9P8}$ is the corrected crosspower without phase mismatch.

The potential energy density can be evaluated as

$$E_P = \frac{1}{2\rho c^2}|P|^2 = \frac{1}{\rho c^2}\,G_{PP}, \tag{44}$$

where G_{PP} is the auto-spectrum of the pressure signal.

3.2. Testing the error sensors

One of the first questions when implementing an ANC application deals with the error sensors that can be applied. The answer to this question frequently depends on the kind of controller that will be implemented. Normally, the filtered-X LMS has no particular problem with error sensors, however the ASIC can have a bad performance if the error sensors are not chosen very carefully.

In order to investigate the performance of the ASIC-PP in the presence of the phase mismatch in the error sensors, two microphone pairs were chosen and analyzed—the phase mismatch between the microphones used in the experiment is shown in Fig. 4. The control results were

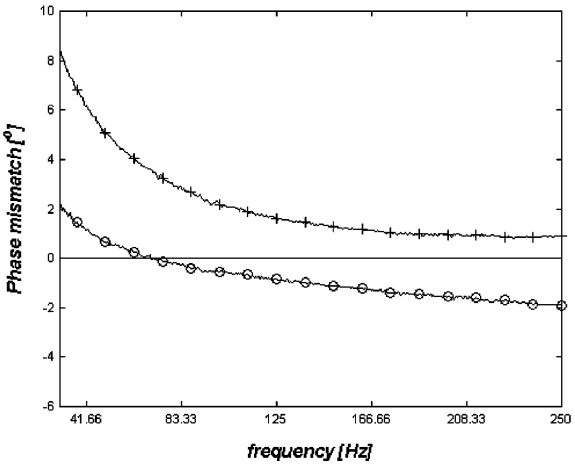

Fig. 4. Phase mismatch between the two microphone pairs: -o-, 1st sensor pair; -+-, 2nd sensor pair.

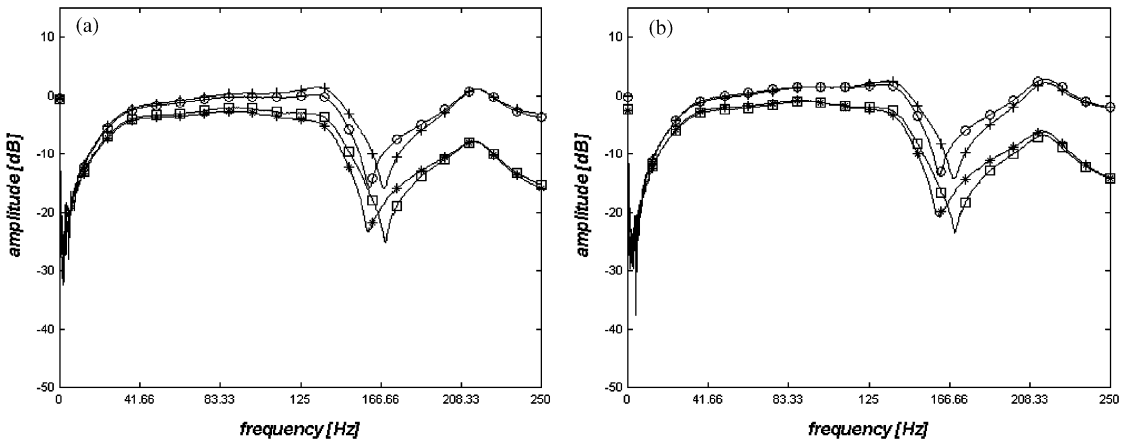

Fig. 5. Frequency response functions (FRFs) of the sensor pairs. (a) 1st microphone pair, (b) 2nd microphone pair. -o-, Z_{P5}; -+-, Z_{P7}; -*-, Z_{S5}; -□-, Z_{S7}.

obtained theoretically using the experimental FRFs (Fig. 5) measured without the presence of the reconstruction filter (Fig. 3). The control results are shown in Fig. 6.

Comparing Figs. 5 (a) and (b), the measured FRFs are nearly the same. Nevertheless, when applying the optimal control law, Eq. (34), results are very different, as shown in Fig. 6(a). The "peaks" in Fig. 6(a) occurred when the denominator of Eq. (34), which is proportional to the sound intensity from the secondary source, is close to zero, as can be observed comparing Figs. 6(a) and (b). Therefore, the best microphone pair to be used as error sensors in the ASIC-PP controller is the 2nd microphone pair because its performance was more uniform than the 1st microphone pair in the whole frequency band of interest.

Fig. 7 shows the phase of the intensity, which is given by the phase angle of the complex term $\mathrm{i}(|Z_{S5}|^2 - Z_{S5}Z_{S7}^* + Z_{S7}Z_{S5}^* - |Z_{S7}|^2)$, for the 1st and 2nd microphone pairs located at positions 5 and 7. It can be noticed that the 2nd microphone pair does not cross the $\pm 90^\circ$ line, which means zero

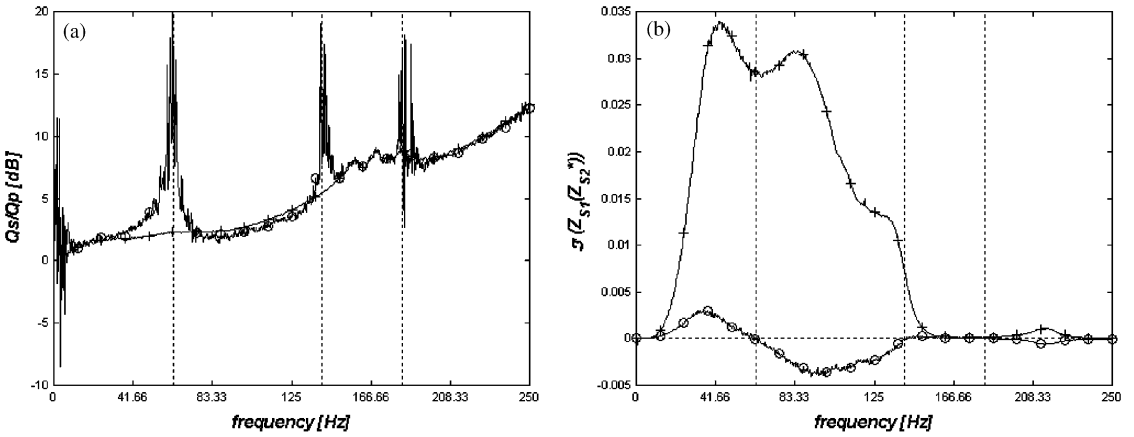

Fig. 6. Comparison of the 1st and 2nd sensor pairs. (a) Theoretical control law of Eq. (34); (b) denominator of Eq. (34). -o-, 1st sensor pair; -+-, 2nd sensor pair.

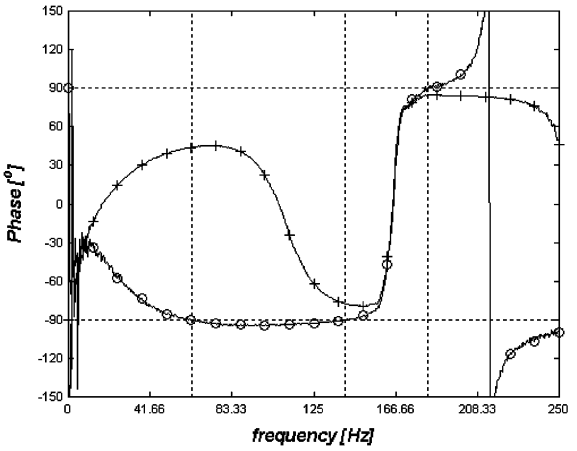

Fig. 7. Sound intensity phase of the error sensors: -o-, 1st sensor pair; -+-, 2nd sensor pair.

active intensity, while the 1st sensor pair does so. This explains why the 1st microphone pair in Fig. 6(b) changes from positive to negative, that means, positive active intensity to negative active intensity due to the phase mismatch. The dotted vertical lines in Figs. 6 and 7 are the points where the denominator of the ASIC-PP, vanishes, which happens at frequencies of approximately 63, 141 and 183 Hz.

The above analysis was applied to the ASIC-PP, but can also be performed for the ASIC-PU, the same final results being expected. It is better to choose a sensor pair that measures a totally positive or totally negative active intensity from the secondary source. The analysis for the ASIC-PU is shown in the next section.

3.3. *Off-line control analyses*

After choosing a suitable pair of sensors (2nd microphone pair in this case), it is necessary to identify the FRFs once more, but now in the presence of the reconstruction filter. In the

experiments performed, the presence of the reconstruction filters did not degrade the estimate of the active intensity because the phase mismatch which they introduced was negligible when compared with the phase mismatch error of the microphones. These FRFs are important both to verify the convergence of the control methods and to implement the methods in real time. In Fig. 8, the FRFs between the sources and the error sensors are shown. It can be noticed that the FRFs for the secondary source are noisy above 160 Hz because of the presence of the reconstruction filter, set to 110 Hz cut-off frequency.

The analysis of the convergence of the ASIC-PU controller can be observed in Fig. 9, where the denominator of Eq. (22) and the sound intensity phase for the P–U approach, i.e., the phase angle of the complex product $Z_{S6}\,Y^{*}_{Z6}$, are shown. It can be noticed in Fig. 9(b) that the phase of the

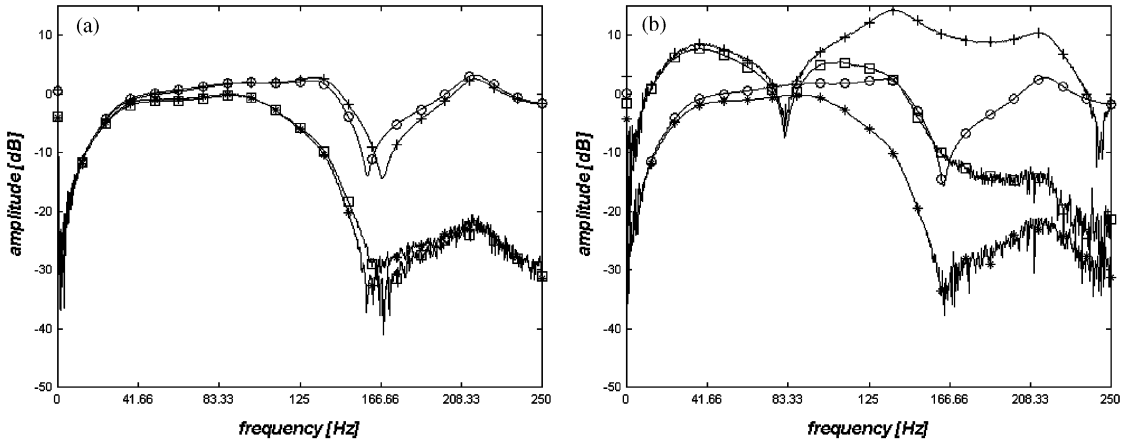

Fig. 8. Frequency response functions (FRFs) between the sources and the error sensors. (a) Error sensors at positions 5 and 7: -o-, Z_{P5}; -+-, Z_{P7}; -*-, Z_{S5}; -□-, Z_{S7}; (b) error sensors at position 6: -o-, Z_{P6}; -+-, Y_{P6}; -*-, Z_{S6}; -□-, Y_{S6}.

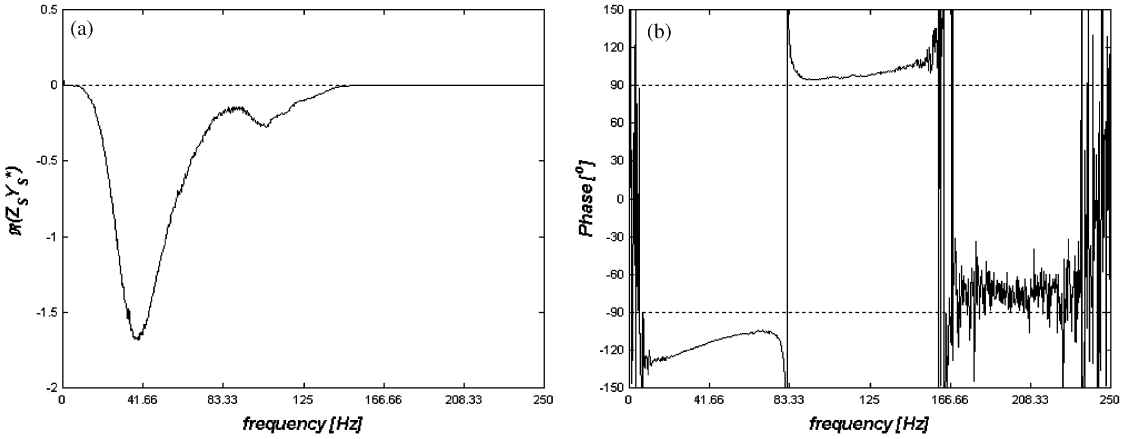

Fig. 9. Analysis of the error sensor for the ASIC-PU controller: (a) denominator of Eq. (22); (b) phase of the sound intensity.

sound intensity did not cross the $\pm 90^\circ$ line, which means zero intensity; thus, the denominator of Eq. (22) did not vanish in the frequency range of interest, Fig. 9(a). Therefore, the sensors of the ASIC-PU can be successfully used in this plane wave field.

The analysis of the convergence of the ASIC-PP controller can be observed in Fig. 10, where the denominator of Eq. (34) and the sound intensity phase for the P–P approach, i.e., the phase angle of the complex term $i(|Z_{S5}|^2 - Z_{S5}Z_{S7}^* + Z_{S7}Z_{S5}^* - |Z_{S7}|^2)$, are shown. It can be noticed in Fig. 10(b) that the phase of the complex intensity did not cross the $\pm 90^\circ$ line (Fig. 10(a)), which means zero active intensity; thus, the denominator of Eq. (34) did not vanish in the frequency range of interest. Therefore, the sensors of the ASIC-PP can be successfully used in this plane wave field.

In Fig. 11 the optimal volume velocities of the secondary source for the different control methods are shown. These optimal volume velocities were evaluated substituting the measured

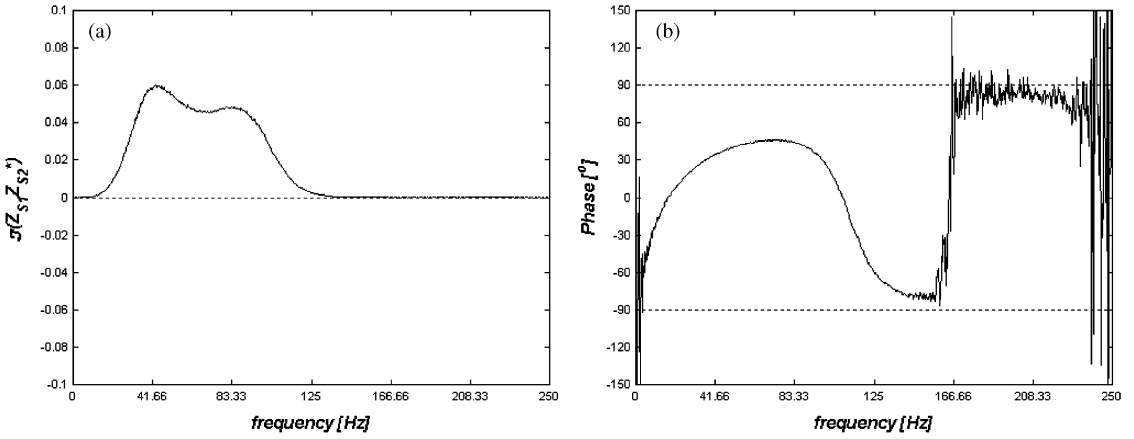

Fig. 10. Analysis of the error sensor for the ASIC-PP controller: (a) denominator of Eq. (34); (b) phase of sound intensity.

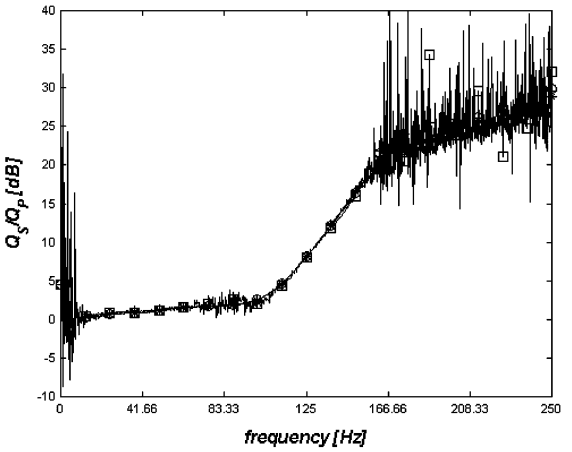

Fig. 11. Optimal volume velocity of the secondary source: -o-, LMS-P; -+-, LMS-U; -*-, ASIC-PP; -□-, ASIC-PU.

FRFs shown in Fig. 8 in Eq. (12) for LMS-P; in Eq. (15) for LMS-U; in Eq. (22) for ASIC-PU; and in Eq. (34) for ASIC-PP. It can be observed that the different control methods yielded nearly the same final result, except for ASIC-PU, which presented more noise in the result. That noise is related to the low signal levels of the FRFs for particle velocity at frequencies around 83.33 Hz, which can be observed in Fig. 8(b).

The four control methods achieved nearly the same final result for the optimal volume velocity Q_S. However, it is known that the active intensity is subject to many errors [14]; it is important to investigate the performance of the ASIC controller under the presence of phase mismatch in order to validate the results presented in Fig. 11.

3.4. Performance analysis of the ASIC under phase mismatch in the error sensors

In order to analyze the performance of the ASIC controller under phase mismatch in the error sensors, a relative phase mismatch in the error sensors is numerically added assuming that

$$\tilde{Z}_{(P,S)5} = Z_{(P,S)5}\mathrm{e}^{\mathrm{i}\theta/2}, \quad \tilde{Z}_{(P,S)7} = Z_{(P,S)7}\mathrm{e}^{-\mathrm{i}\theta/2} \tag{45}$$

for the ASIC-PP and

$$\tilde{Z}_{(P,S)6} = Z_{(P,S)6}\mathrm{e}^{\mathrm{i}\theta/2}, \quad \tilde{Y}_{(P,S)6} = Y_{(P,S)6}\mathrm{e}^{-\mathrm{i}\theta/2} \tag{46}$$

for the ASIC-PU.

The results are compared using the attenuation in the active intensity estimated with the error sensors without phase mismatch (i.e., the "actual" active intensity) obtained using the control law computed by the ASIC controller using the signals with phase mismatch error. The phase mismatch was varied in the range $\pm 90^\circ$.

The results in the attenuation of the active intensity are shown in Fig. 12 for the ASIC-PP and in Fig. 13 for the ASIC-PU. The divergence regions in Figs. 12 and 13 represent the regions where the denominator of the ASIC controller expression vanishes due to the phase mismatch error, i.e., $\Im\{Z_{S5}Z_{S7}^{*}\mathrm{e}^{\mathrm{i}\theta}\} = 0$ for the ASIC-PP and $\Re\{Z_{S6}\,Y_{S6}^{*}\mathrm{e}^{\mathrm{i}\theta}\} = 0$ for the ASIC-PU. As mentioned in

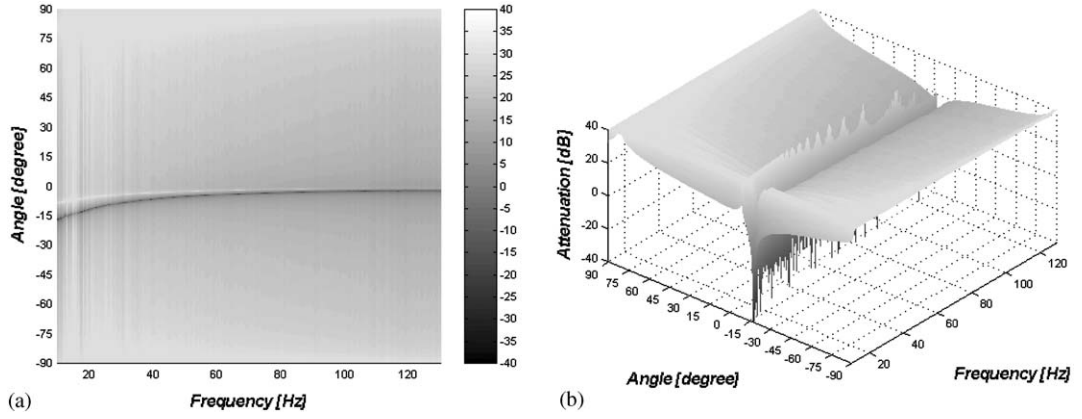

Fig. 12. Attenuation in the "actual" active intensity measured by the error sensors for the ASIC-PP controller: (a) 2-D view; (b) 3-D view.

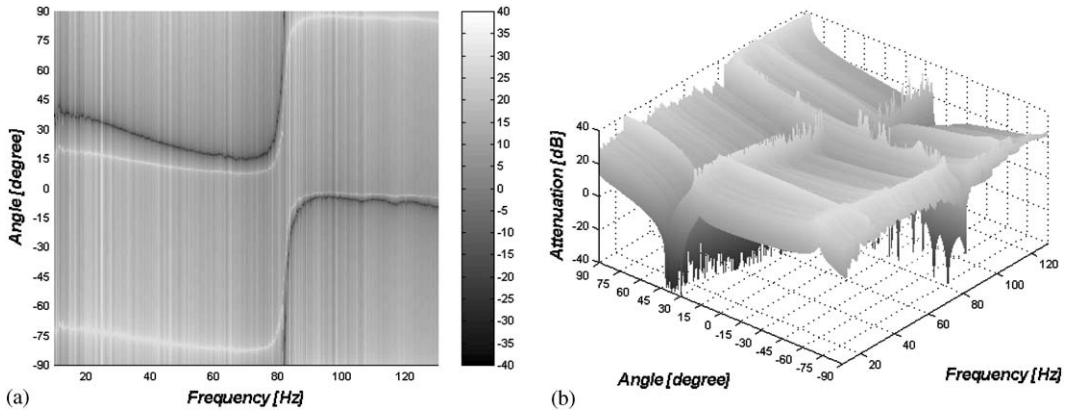

Fig. 13. Attenuation in the "actual" active intensity measured by the error sensors for the ASIC-PU controller: (a) 2-D view; (b) 3-D view.

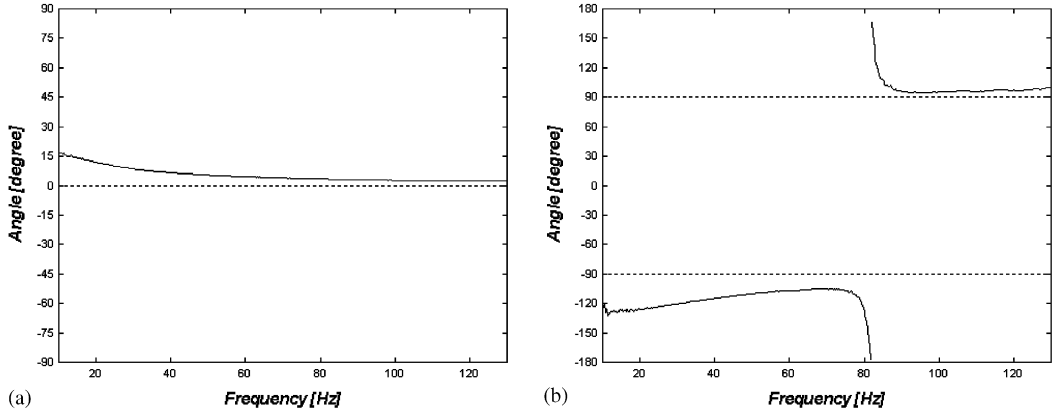

Fig. 14. Angle of the complex product: (a) $Z_{S5}Z_{S7}^{*}$, and (b) $Z_{S6}Y_{S6}^{*}$.

Sections 2.5 and 2.6, the vanishing of the denominator means that the measured intensity cannot be controlled by the actuator (lack of controllability).

This fact can be better understood using Fig. 14 where the angles of the complex products $Z_{S5}Z_{S7}^{*}$ and $Z_{S6}Y_{S6}^{*}$ are shown. The denominator of the ASIC-PP goes to zero when the imaginary part of $Z_{S5}Z_{S7}^{*}$ vanishes; the zero dashed line in Fig. 14(a). Thus, when a relative phase mismatch is added in the error sensors driving the angle of $Z_{S5}Z_{S7}^{*}$ to zero, the ASIC-PP becomes unstable. The same fact occurred with ASIC-PU, where the denominator vanishes when the real part of $Z_{S6}Y_{S6}^{*}$ is close to zero, i.e., the solid curve is close to the $\pm 90^{\circ}$ dashed lines in Fig. 14(b).

The angles shown in Fig. 14 are characterized by the acoustic field, in this case the duct, and by the pre-existing phase mismatch in the error sensors. In previous works [2,4], matched-phase sensors were used to avoid this problem and the issue was not addressed.

3.5. Energetic analysis

Once the off-line investigations were finished, and the error sensors and the control method performances were defined, the real-time implementations, where the control methods were developed in Matlab/Simulink and implemented in a dSPACE 1102 control board could be started. The acoustic power radiated from the sources, the active intensity, and the potential energy density were measured with the control on and off.

In Fig. 15, the changes in the volume velocity of the primary source can be observed. It can be noticed that the control methods change the volume velocity of the primary source slightly, the changes being basically the same for the four methods.

The ratios between the acoustic power radiated from the sources with the controller on and off is shown in Fig. 16. Fig. 16(a) shows the attenuation in the power radiated by the primary source. It can be observed that, although the ASIC-PP achieved the best radiated power attenuation at 41.66 Hz, it achieved one of the worst results at 83.33 Hz. However, the active control methods effectively decreased the radiated acoustic power from the primary source in the controlled frequency range (41.66, 83.33 and 125 Hz). Fig. 16(b) shows the ratio between the acoustic power radiated by the secondary source and the acoustic power radiated by the primary source working alone. The results show that the secondary source radiated less acoustic power than the primary source working alone in the controlled frequency range (41.66, 83.33 and 125 Hz).

It is import to notice that the control methods were implemented at different times. So, some variation in the radiated acoustic power is expected (this variation is caused by small changes in the gain of the power amplifier and environmental changes). Furthermore, the secondary source acts like a passive absorber when the controller is off.

The acoustic power radiated by the primary source was attenuated. Therefore, it is expected that the active intensity was attenuated too, but the secondary source is still radiating some acoustic power. So, the best way to observe what is happening with the energy in the duct is observing the active intensity.

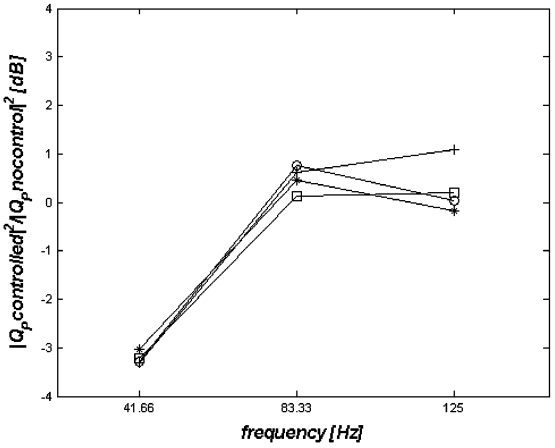

Fig. 15. Change in the experimental volume velocity of the primary source caused by the controller. -o-, LMS-P; -+-, LMS-U; -*-, ASIC-PP; -□-, ASIC-PU.

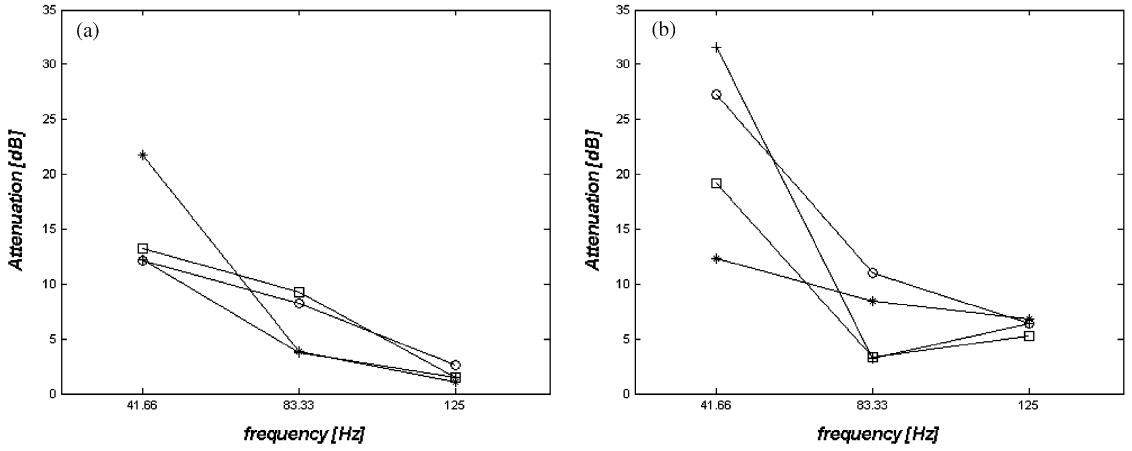

Fig. 16. Attenuation in the radiated acoustic power W_R. (a) Primary source power attenuation; (b) power radiated by the secondary source relative to the power radiated by the primary source alone. -o-, LMS-P; -+-, LMS-U; -∗-, ASIC-PP; -□-, ASIC-PU.

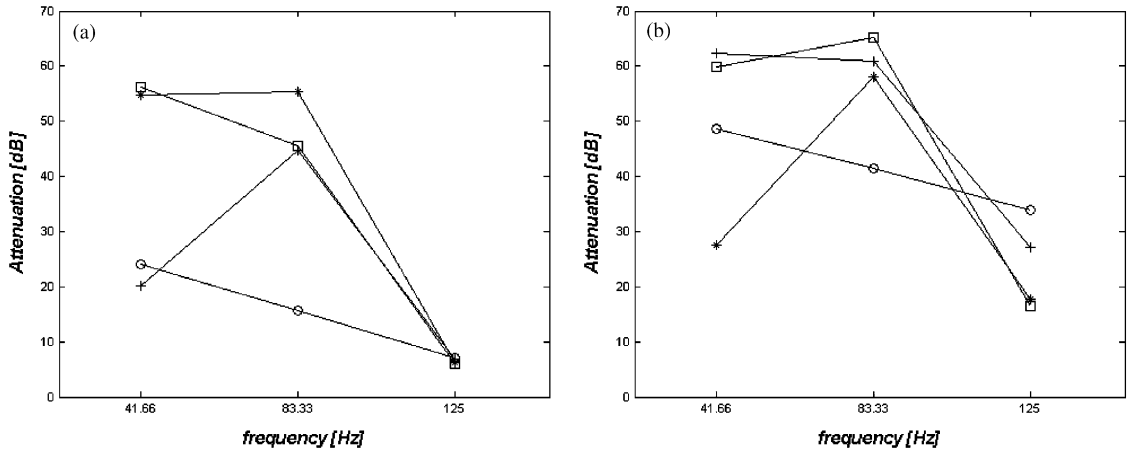

Fig. 17. Attenuation in the active intensity I_A measured (a) between the error sensors at positions 2 and 3, (b) between the error sensors at positions 8 and 9. -o-, LMS-P; -+-, LMS-U; -∗-, ASIC-PP; -□-, ASIC-PU.

Fig. 17 shows the attenuation in the active intensity. A significant attenuation is obtained when the control methods are applied. Comparing Figs. 17(a) and (b), it can be observed that the active intensity in the duct was attenuated both upstream and downstream from the secondary source in the controlled frequency range (41.66, 83.33 and 125 Hz).

This investigation allowed the observation of what happens with the energy flow in the duct before and after the control methods are applied. Nevertheless, for a more complete understanding of the control phenomena, it is also important to observe the distribution of the potential energy density in the duct before and after the control is acting.

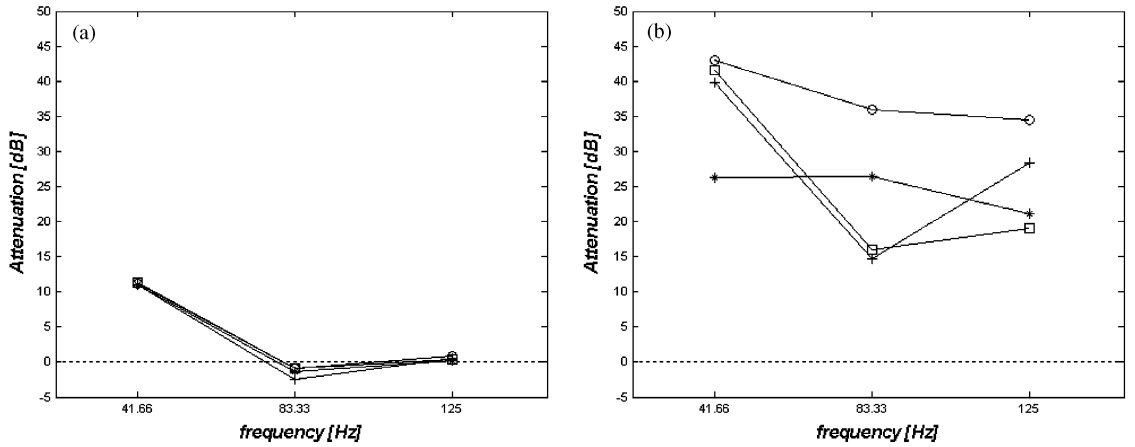

Fig. 18. Attenuation in the potential energy density E_P measured at (a) position 2, (b) position 8. -o-, LMS-P; -+-, LMS-U; -*-, ASIC-PP; -□-, ASIC-PU.

Another interesting observation about Fig. 17 is that the active intensity attenuation exhibits larger differences for the different controllers than the acoustical potential energy. As expected, the intensity controllers caused a larger attenuation of the active intensity, while the controller using the pressure error signal caused a larger attenuation of the acoustic potential energy.

In Fig. 18 the distribution of the potential energy density relative to the position of the secondary source is shown. It can be noticed that the potential energy is changed but not attenuated upstream from the secondary source while it is heavily attenuated downstream.

It is interesting to observe in Fig. 18(b) that the attenuation of the acoustic potential energy changes with the control method and with the controlled frequency component. Moreover, the best result was obtained by the LMS-P, which used the microphone as an error sensor.

4. Conclusions

Four active noise control methods were implemented in a one-dimensional acoustic waveguide. The four methods are the frequency-domain filtered X LMS based upon controlling potential energy density and kinetic energy density and the active sound intensity control (ASIC) based upon controlling active intensity with the P–U and P–P approaches. The results showed that the methods achieved basically the same final result in all criteria observed, i.e., the minimization of the radiated acoustic power, the minimization of the active intensity and the minimization of the potential energy density. Furthermore, as expected [4], in the controlled case there is less energy flow than in the uncontrolled case, i.e., the sources radiated less acoustic power when working simultaneously than the primary source radiated when working alone (uncontrolled case).

It was observed that, provided the secondary source can produce a non-negligible active intensity at the location where the error sensors are placed, i.e., the plant is controllable, the ASIC is robust relative to phase mismatch errors.

Besides, it was shown that the particle velocity sensor can be successfully used as an error sensor in ANC application. It is an alternative to microphones and, when used, the cost function can either be the active intensity or the kinetic energy density.

References

[1] S.D. Sommerfeldt, P. Nashif, An adaptive filtered-X algorithm for energy-based active control, *Journal of the Acoustical Society of America* 96 (1) (1994) 300–306.

[2] S.W. Kang, Y.H. Kim, Active intensity control for the reduction of radiated duct noise, *Journal of Sound and Vibration* 201 (5) (1997) 595–611.

[3] X. Qiu, C.H. Hansen, An adaptive sound intensity control algorithm for active control of transformer noise, *Proceedings of the Fifth International Congress of Sound and Vibration*, Adelaide, Australia, 1997, pp. 205–212.

[4] D.C. Swanson, S.M. Hirsch, K.M. Reichard, J. Tichy, Development of a frequency-domain filtered-X intensity ANC algorithm, *Applied Acoustics* 57 (1) (1999) 39–49.

[5] J.R.F. Arruda, W. Dehandschutter, P. Sas, Strategies for active vibration control using a power flow approach, *Acta Acustica* 84 (3) (1998) 465–474.

[6] S. Haykin, *Adaptive Filter Theory*, 3rd Edition, Prentice-Hall, Englewood Cliffs, NJ, 1996.

[7] A.K.A. Pereira, K.M. Ahmida, J.F.R. Arruda, Active vibration control using a generalized intensity controller, *Proceedings of Active 99*, Ft. Launderdale, FL, 1999, pp. 1035–1046.

[8] L.V. Donadon, J.R.F. Arruda, Theoretical comparison of active noise control using potential energy error sensing and intensity error sensing, *Proceedings of Internoise 2000*, Leuven, France, 2000.

[9] C.F.N. Cowan, Performance comparisons of finite linear adaptive filters, *IEE Proceedings part F* 134 (3) (1997) 211–216.

[10] L.E. Kinsler, A.R. Frey, A.B. Coppens, J.V. Sandres, *Fundamentals of Acoustics*, Wiley, New York, 1982.

[11] B. Widrow, S.D. Stearns, *Adaptive Signal Processing*, Prentice-Hall, Englewood Cliffs, NJ, 1985.

[12] X. Qiu, C.H. Hansen, X. Li, A comparison of near-field acoustic error sensing strategies for the active control of harmonic free field sound radiation, *Journal of Sound and Vibration* 215 (1) (1998) 81–103.

[13] Y.C. Park, S.D. Sommerfeldt, Global attenuation of broadband noise fields using energy density control, *Journal of the Acoustical Society of America* 101 (1) (1997) 350–359.

[14] F.J. Fahy, *Sound Intensity*, 2nd Edition, E&FN Spon, London, 1995.

[15] L.V. Donadon, Analytical and Experimental Analysis of Active Noise Control Strategies, Ph.D. Dissertation, University of Campinas, Brazil, 2002.

[16] J.F.R. Arruda, W. Dehandschutter, P. Sas, Active vibration in finite plates using a structural power flow approach, *Acta Acustica* 83 (1997) 465–474.

[17] J.R.F. Arruda, A.K.A. Pereira, Intensity methods for noise and vibration analysis and control, *Proceedings of International Symposium on Dynamic Problems in Mechanics and Mechatronics—EUROdinmame99*, Reisenburg, 1999.

[18] H.E. Bree, P. Leussink, T. Korthorst, H. Jansen, T. Lammerink, M. Elwenspoek, The microflown: a novel device measuring acoustical flows, *Sensors and Actuators* 54 (1996) 552–557.

[19] F.J.M. Eerden, H.E. Bree, H. Tijdeman, Experiments with a new acoustic particle velocity sensor in an impedance tube, *Sensors and Actuators* 69 (1998) 126–133.

[20] H.E. Bree, W.F. Druyvesteyn, M. Elwenspoek, Realization and calibration of a novel half inch P-U sound intensity probe, *Proceedings of 106th AES*, Munich, 1999.

[21] H.E. Bree, An overview of microflown technologies, *Acta Acoustica* 89 (2003) 163–172.

[22] C.H. Hansen, S.D. Snyder, *Active Control of Noise and Vibration*, E&FN Spon, London, 1997.

[23] J.Y. Chung, Cross-spectral method of measuring acoustic intensity without error caused by instrument phase mismatch, *Journal of the Acoustical Society of America* 64 (6) (1978) 1613–1616.

[24] F. Jacobsen, A note on the accuracy of phase compensated intensity measurements, *Journal of Sound and Vibration* 174 (1) (1994) 140–144.